Research Article

Design Study for a Quasisynchronous CDMA Sensor Data Collection System: An LEO Satellite Uplink Access Technique Based on GPS

Yijun Chen,[1,2] Sheng Ding,[2] Zhouchen Xie,[2] Zhuangping Qi,[2] and Xuwen Liang[1,2]

[1]*Shanghai Institute of Microsystem and Information Technology, Chinese Academy of Sciences, Shanghai 200050, China*
[2]*Shanghai Engineering Center for Microsatellites, Chinese Academy of Sciences, Shanghai 201203, China*

Correspondence should be addressed to Xuwen Liang; 18217631362@163.com

With the development of the LEO satellite communication technology, highly dependable wireless communication and sensor data collection using LEO satellites have been getting much attention for emergency, marine research, and forest fire disaster in the remote region. The satellite system is expected to have the following features: rapid production, low cost, and fast construction of the satellite network. In this paper, a QS-CDMA uplink access technique in the LEO satellite is presented and discussed, which is focused on the local clocks using GPS 1PPS timing signals and the Doppler compensation for terminal uplink. The spreading code with length of 1023, which is used for the uplink preamble, selects the shift-m-sequence that can greatly reduce the MAI and increase the number of simultaneous access users. A novel analysis method for the accuracy of clock synchronization and a novel method for the estimation of Doppler shift and propagation delay are presented. These methods are used to guide the specific hardware implementation of the QS-CDMA LEO satellite sensor data collection system. Through simulations and experiments, it results in that this system structure can drastically reduce the complexity in implementing the acquisition in the satellite and increase the adaptability of the satellite system in different environments.

1. Introduction

When great disaster occurs, such as earthquake, many terrestrial infrastructures are seriously damaged. We had to take several days to get disaster situation and confirm safety of victims. So we expect that a satellite system provides a minimum reliable connection. The satellite system should have some disaster response features such as safety confirmation and position report. In marine research, oceanographic buoy can transmit information from the submerged nodes, which consist of sensors, to the remote ground station. When forest fire disaster happened in the remote region, the fire sensor transmits alert to the satellite and the satellite forwards the information to the nearest monitor station which maybe a hundred kilometers away. Meanwhile, many different kinds of sensors can collect the information of the forest such as temperature, humidity, and trespass. The satellite system should have some data collection features such as data store

and forward. Nowadays the further development of satellite communication has been assisting a very high competition for the discovery of advanced technologies, which have demanded service to support more users and low complexity for satellite payload. In order to collect information of the disaster region in time, the modern trend in Low Earth Orbit (LEO) satellite communications system has to provide reliable short message communication to a large number of user terminals and sensors. An access technique for band-limited quasisynchronous CDMA (BLQS-CDMA) has been proposed in [1], and the network reference clock and frequency are transmitted embedded in the CDMA signal structure using a dedicated code, which is called master code. In [1], the preferentially phased Gold sequences are optimal for BLQS-CDMA with maximum timing jitter of $\pm 0.5 \cdot T_c$, where T_c is the code duration. The possibility of keeping the timing error below 0.3 chips in the worst dynamic case for a chip rate of about 1 Mchip/s has been

demonstrated. However, the network control station is hard to construct for marine research in the middle of ocean. Meanwhile, with the increasing of user requirements for data rate and the number of simultaneous access users, the Gold sequences cannot satisfy these requirements, because the higher date rate is, the more stringently the requirements for timing jitter are. The more simultaneous access users are, the worse the performance of BER is, a situation caused by the cross-correlation of the Gold sequence. The satellite wide-band CDMA consists of synchronous downlink and quasisynchronous uplink [2]. The system also requires the Base Station to synchronize system clock. A slotted quasisynchronous CDMA access system has been proposed in [3], and the prime application of the system is short message services. The slotted QS-CDMA system requires the control earth station to provide accurate slot synchronization reference. In [1–3], previous research had not provided analysis method for the accuracy of clock synchronization and just made a request for system synchronization. Previous research had not provided estimation and analysis method for Doppler shift and propagation delay either.

The modern trend in digital communications is to synchronize with the local time, whose synchronous errors arise from different allowed uncertainties in communication systems. Global Positioning System (GPS) receivers are used by conveying the reference time to the locked-clock loop via the one-pulse-per-second (1PPS) output. It was noticed that the average time error produced by the receivers varied over a range of about 150 nanoseconds (ns) in 2002 [4]. The current production as published showed that jumps are at the 10 ns level [5]. An optimal synchronization of local clocks by GPS one-pulse-per-second (1PPS) timing signals is specified in [6], which use predictive FIR filter. The application of Kalman filter for clock synchronization is proposed in [7]. Nowadays the clock synchronization technique based on GPS has reached a high degree of accuracy.

Generally, in severe Doppler environment, such as the LEO satellite communication, the pseudorandom (PN) code acquisition for the direct-sequence spread spectrum (DSSS) communication is hard to accomplish. The existence of carrier and code Doppler results in a prolonged acquisition process, and it also increased hardware complexity due to the need for a two-dimensional (chip delay and frequency) search structure of code and carrier synchronization. The Doppler characterization for LEO satellites is analyzed in [8]. The direct-sequence spread spectrum code acquisition in the presence of Doppler shift was investigated in [9]. In [10], Doppler compensation loop structure was proposed. In [9, 10], some algorithms have been used to compensate for the Doppler shift by satellites. Due to low-power consumption, which is characteristic of LEO satellites, the acquisition and synchronization structure should meet the requirements of decreasing hardware complexity. At the same time, the satellites need to serve as many users as possible, but the complexity of hardware implementation will limit the number of users.

In this paper, we propose a novel quasisynchronous CDMA (QS-CDMA) transmission scheme based on GPS to increase system capacity, decrease hardware complexity of

TABLE 1: System parameters.

Parameters	Range
Orbital altitude	1000 km
Carrier center frequency	1.5 GHz
PN code length (preamble)	1023
Data bit rate	5 kHz
Code chip rate	5.115 MHz
Carrier Doppler shift range	±31.68 kHz
Maximal carrier Doppler rate	233 Hz

satellites, provide reliable short message service, and collect data from sensors. The starting point is to analyze the feasibility of implementing local clocks using GPS 1PPS for LEO satellites and terminals. The results will be used to specify the accuracy of clock synchronization. Due to the extremely high Doppler that is an important characteristic of LEO satellites, the acquisition of satellites is significantly simplified by using a continuous wave downlink pilot for uplink carrier Doppler estimation and compensation. The results are shown with the acquisition time performance of satellites that is considerably improved, the number of users is significantly increased and the anti-interception ability is improved. The following sections of this paper are organized as follows: Section 2 describes the overall system architecture and requirements, Section 3 depicts a novel analysis method for accuracy of the clock synchronization technique based on GPS, a novel method of carrier Doppler compensation, propagation delay estimation, and a receiver scheme of satellite, Section 4 introduces the simulation and experiment results, and Section 5 introduces the implementation results and gives a brief conclusion.

2. System Structure and Requirements

2.1. System Structure

2.1.1. System Parameters. The LEO satellite system being considered has the parameters shown in Table 1.

The main differences among QS-CDMA proposed in this paper, BLQS-CDMA in [1], and slotted QS-CDMA in [3] are shown in Table 2.

From Table 2, we can know that, the synchronization reference provided by the control station is complex in the middle of ocean. Therefore, synchronization reference provided by GPS receiver is wide applicability.

In Figure 1, the system of interest includes an LEO satellite, a large number of user terminals, sensors, and the GPS system. The LEO satellite broadcasts a continuous pilot carrier for downlink acquisition, tracking, uplink Doppler estimation, and compensation. A high-precision single GPS receiver is required by the LEO satellite. User terminal consists of a GPS receiver chip that offers 1PPS output, a local oven-controlled crystal oscillator (OCXO), or temperature compensated crystal oscillator (TCXO) which is used to form the local time scale with a high-resolution divider, baseband processing module, and so on.

TABLE 2: System comparison.

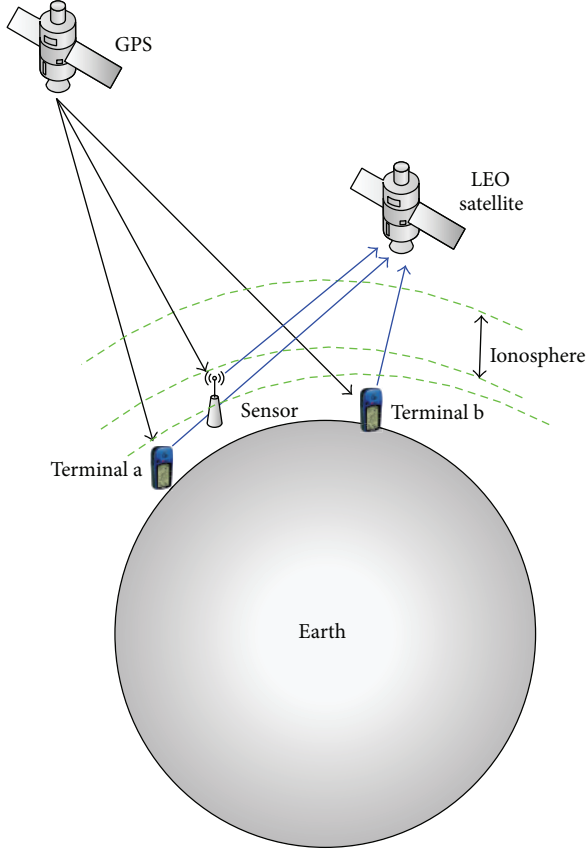| Difference	System		
	QS-CDMA	BLQS-CDMA	Slotted QS-CDMA
(1) Synchronization reference	Provided by GPS receiver	Provided by the nation control center station	Provided by the control earth station
(2) Spreading codes	Shift-m-sequence	Gold sequence	Unspecified

FIGURE 1: System structure.

TABLE 3: Main parameters of access procedure.

Parameters	Definition
Δt_k	The total time error of the 1PPS provided by GPS receiver of satellite and terminal k
R_k^{down}	The downlink propagation distance between satellite and terminal k
R_k^{up}	The uplink propagation distance between satellite and terminal k
t_k^{down}	The time that the terminal k receives the downlink pilot
t_k^{up}	The time that the terminal k transmits the uplink signal
f_c^{down}	The downlink carrier frequency
f_c^{up}	The uplink carrier frequency

FIGURE 2: QS-CDMA access technique flow diagram.

2.1.2. System Synchronization Reference.

We expect to reduce the complexity and the expense of the QS-CDMA system and increase the adaptability of the system. With the technology development, GPS receiver chip is cheaper and consumes less power. In this paper, GPS receiver should provide accurate synchronization reference. Nowadays the clock synchronization technique based on GPS has reached a high degree of accuracy. So 1PPS signal can meet the requirements. The local clock of the LEO satellite and all user terminals should be aligned with 1PPS as reference. The analysis of the system time synchronization error will be discussed in Section 3.

2.1.3. Doppler Shift, Propagation Delay Compensation, and Access Procedure.

For QS-CDMA access, some main parameters are defined in Table 3. The flow diagram with the proposed access technique is shown in Figure 2.
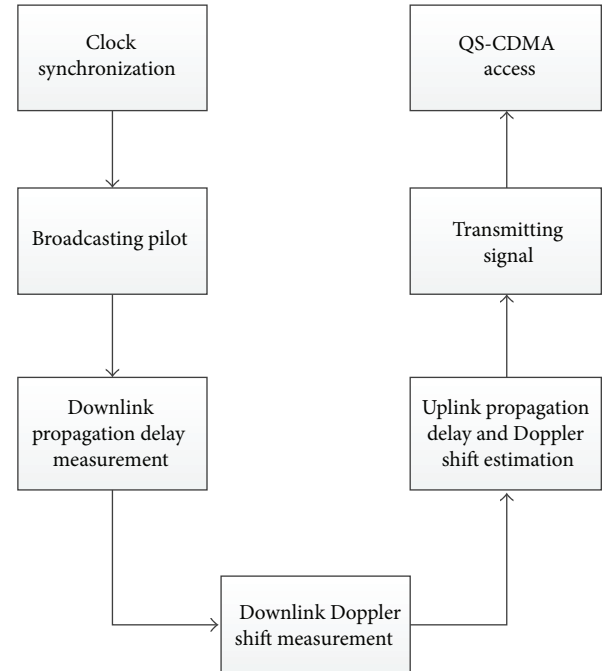
In Figure 2, the QS-CDMA access technique flow diagram can be divided as follows:

(a) Clock synchronization: The local clocks of the LEO satellite and all user terminals align with 1PPS as reference.

(b) Broadcasting pilot: After achieving clock synchronization, the LEO satellite broadcasts a downlink continuous pilot. The pilot frame header aligns with the 1PPS of
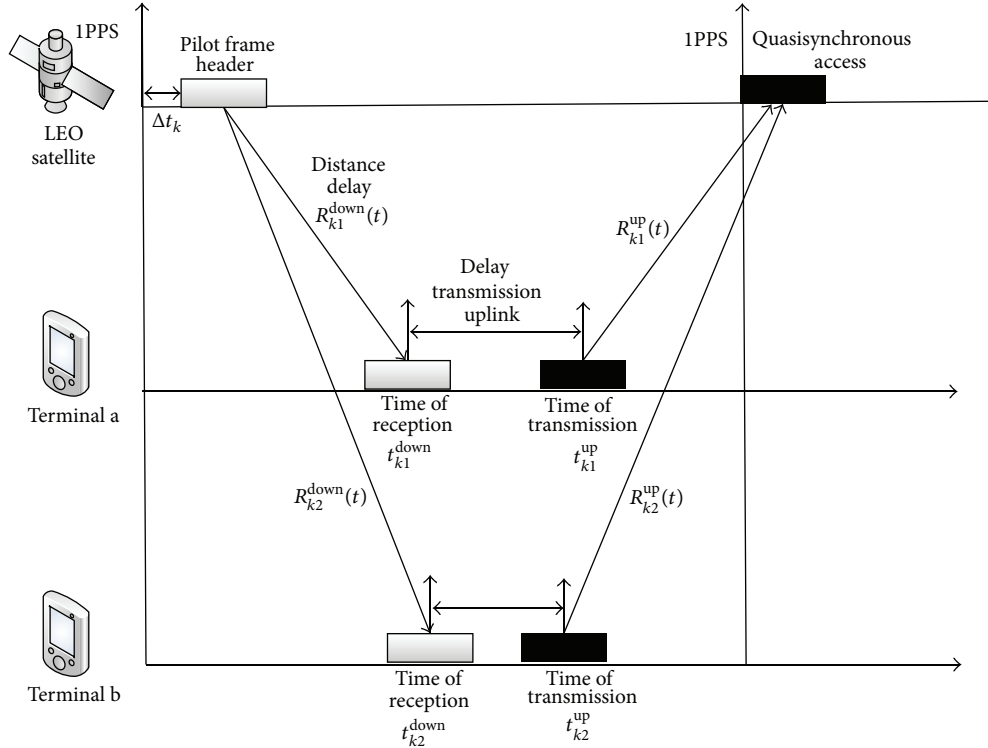
FIGURE 3: QS-CDMA delay compensation based on GPS timing diagram.

the satellite, which is used to assist terminals in measuring downlink propagation delay R_k^{down}.

(c) Downlink propagation delay measurement: Through 1PPS of terminal and the time of pilot frame header reception t_k^{down}, the terminal measures and computes R_k^{down} that operates at a 40 MHz clock speed. It should be noted that the time length of the pilot frame header, which is demodulated by the terminal receiver, varies with the Doppler shift.

(d) Downlink Doppler shift measurement: The terminal measures the downlink carrier Doppler shift and code Doppler shift by the acquisition module and the tracking loop of the terminal receiver. The acquisition module provides the initial Doppler shift. The tracking loop updates Doppler shift in real time.

(e) Uplink propagation delay and Doppler shift estimation: The terminal estimates uplink carrier Doppler shift, code Doppler shift, and uplink propagation delay R_k^{up} through downlink carrier Doppler shift, which is updated by the receiver tracking loop in real time.

(f) Transmitting signal: The terminal transmits signals R_k^{up}/c before next 1PPS.

(g) QS-CDMA access: At the beginning of next satellite 1PPS, the satellite receives all the uplink signals which achieve QS-CDMA access.

In Figure 3, Δt_k consists of the time error of the 1PPS produced by GPS receivers of satellite and terminal k. Firstly through downlink continuous pilot carrier, 1PPS of the terminal, and t_k^{down}, the terminal should easily compute downlink propagation delay R_k^{down}. Secondly, it utilizes

the pilot to measure the downlink carrier Doppler shift and code Doppler shift at this point. Thirdly, the uplink carrier Doppler shift will be estimated through downlink Doppler shift and the frequency ratio between downlink carrier frequency and uplink carrier frequency. Then R_k^{up} and uplink carrier Doppler shift will be used to compensate uplink propagation delay and Doppler shift. Finally, the terminals transmit signals at t_k^{up} before next 1PPS, and at the beginning of 1PPS, and the satellite will receive all the uplink signals which achieve QS-CDMA access. The QS-CDMA access process of sensors is similar to user terminals. The user terminals and sensors can use the same communication module.

2.1.4. Spreading Code for QS-CDMA. Through QS-CDMA access, multiple-access interference (MAI) will be obviously decreased. Selecting the appropriate spreading codes is also important. We proposed that the uplink preamble of the system selects shift-m-sequence whose code length is 1023. The m-sequences possess the following three properties: the balance property, the run property, and the correlation property [11]. If a complete sequence is compared bit-by-bit with any shift of the same sequence, the number of agreements minus the number of disagreements is always −1; that is, there is one more disagreement position than the number of agreement positions. Exploitation of the correlation property of PN sequences makes it possible to design direct sequence spread-spectrum (DSSS) systems.
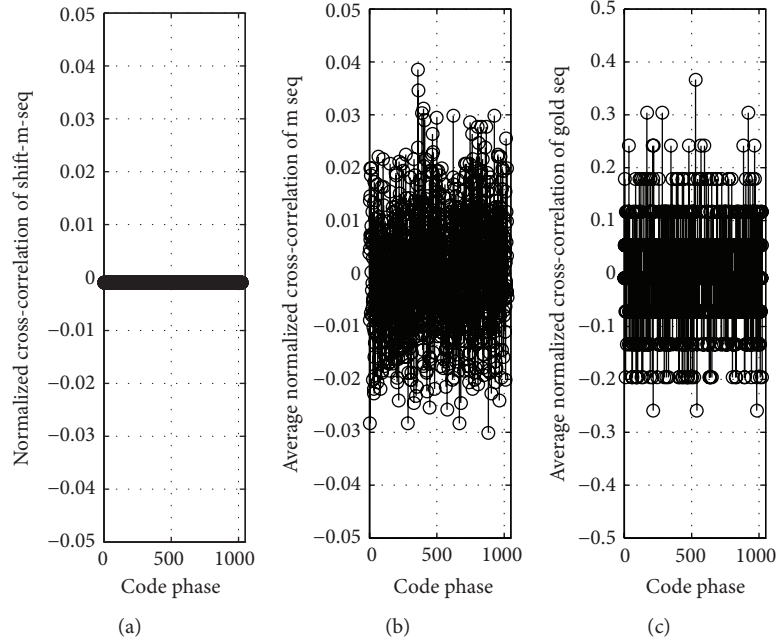
Figure 4: Normalized cross-correlation performance.

Table 4: m-sequence parameters.

User number	Primitive polynomial (decimal)
1	1033
2	1051
3	1063
4	1069
5	1125
6	1135
7	1153
8	1221
9	1239
10	1255

We compare the cross-correlation performance of different m-sequences, whose primitive polynomials are shown in Table 4. We also compare the cross-correlation performance of different Gold sequences whose code length is 1023. We assume that the code phase difference of shift-m-sequence, m-sequences, and Gold sequences is an integer. Normalized cross-correlation is shown in Figure 4.

From Figure 4(a), we can see that the normalized cross-correlation of shift-m-sequences, whose primitive polynomials are 1033, is 9.8×10^{-4}. From Figure 4(b), we can see that the average normalized cross-correlation of the m-sequences, whose primitive polynomials are shown in Table 3, is about 0.04. From Figure 4(c), we can see that the average normalized cross-correlation of the Gold sequences, which is a total of ten sequences, is about 0.3. That is

the value of m-sequences about 10 times. The cross-correlation performance of shift-m-sequence is much better than the Gold sequence. Thus the number of simultaneous access users that use shift-m-sequence is much more than the number of simultaneous access users that use Gold sequence.

Due to the correlation property of m-sequence, the cross-correlation performance of shift-m-sequence is superior. Because any shift-m-sequence is shifted by the same m-sequence, it cannot be acquired in A-CDMA system. However, shift-m-sequence can be used in QS-CDMA system. Every user selects a shift-m-sequence that is different from initial code phase and the code phase interval between one user and the other is greater than or equal to 1 chip. Therefore, through QS-CDMA access with shift-m-sequence, MAI will be obviously decreased.

Theoretically, the QS-CDMA system uses a group of m-sequences whose code length is 1023 and can only provide service to 60 users at one time. The reason is that there are only 60 primitive polynomials for m-sequences with length of 1023. The QS-CDMA system uses a group of shift-m-sequences whose code length is 1023 and can provide service to 1023 users at one time. However, if the code offset of shift-m-sequence is within ±1 code epoch, in order to avoid the self-interference of shift-m-sequences, the number of users is only 341. It means that the smaller code offset is, the more users will be got. Thus, Section 3 will depict a novel method for accuracy of the clock synchronization technique and a novel method of Doppler compensation.

2.2. System Requirements. In order to reduce the LEO satellite implementation complexity and the multiple-access interference (MAI), the system requires limiting the carrier Doppler shift to be within ±0.5 Rb, where Rb is the bit rate of data,

Pilot frame header	PN code indication	Contents

(a)

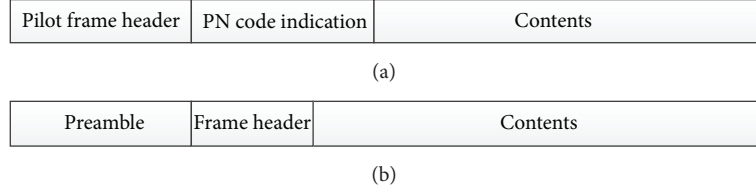| Preamble	Frame header	Contents

(b)

FIGURE 5: Frame structure: (a) downlink pilot structure, (b) uplink data structure.

TABLE 5: Requirements for the code offset.

Code rate	Maximum tolerable code offset
10.23 MHz	97.75 ns
5.115 MHz	195.50 ns
4.092 MHz	244.38 ns
2.046 MHz	488.76 ns

FIGURE 6: Local clock synchronization block diagram.

and the code offset to be within ±1 code epoch at 5 million chips per second (Mchip/s). By assuming that the proposed Doppler compensation meets the requirements, acquisition structure is demonstrated to be feasible with acceptable acquisition time by a 1-dimensional serial search instead of the considerably longer 2-dimensional search that will be required in the uncompensated case.

The requirements for the code offset in different code rate are shown in Table 5.

From Table 5, it is shown that the higher code rate is, the more stringently the requirement for code offset is.

3. Implementation Architecture and Performance Analysis

In this section, the key features of the QS-CDMA access technique will be studied in depth. Through the 1PPS, all users that use random spread spectrum codes employ slotted ALOHA (S-ALOHA) random access protocol. The pilot broadcasts the codes which collided with each other, and then the users repeat to transmit with spread spectrum random codes at next 1PPS or next slot.

3.1. Downlink Pilot and Uplink Preamble Frame Structure. Downlink pilot structure consists of pilot frame header, PN code indication, and contents. The pilot frame header is aligned with 1PPS of satellite and used for all user acquisition. The PN code indication denotes the codes which collided with each other (see Figure 5).

Uplink structure consists of preamble, frame header, and contents. The preamble is also aligned with 1PPS of terminal and is used for satellite acquisition. The frame header indicates the beginning of the contents.

All user terminals select a shift-m-sequence from a group of sequences, whose code length is 1023, for the uplink preamble of the system. Because of QS-CDMA access technique, the code phase of preamble should be predefined,
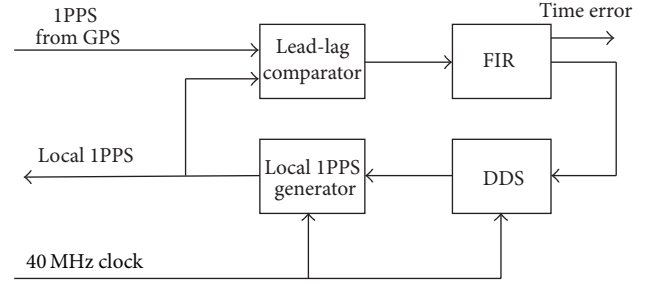
so the acquisition of satellite will be easy to capture the signals from terminal, and the time of preamble should be shortened. The short preamble which is spread by shift-m-sequence will increase ability to anti-intercept. Meanwhile, the shorter the preamble is, the more system capacity we will obtain.

3.2. Analysis of Clock Synchronization Time Error Based on GPS. In this paper, we assume that the average time error of the 1PPS produced by GPS receivers of satellite varied over a range of about 10 ns and 100 ns by terminal receivers. Nowadays, these errors are common errors and the ranges can be easy to be achieved [5]. The local clock synchronization block diagram is shown in Figure 6.

In Figure 6, we can see that the lead-lag comparator compares the 1PPS from GPS receiver and the local 1PPS. Through finite impulse response (FIR), the time error drives the direct digital synthesizer (DDS) to generate frequency control word. Finally, the local 1PPS generator provides the local 1PPS at a 40 MHz work clock.

Some main analysis parameters are defined in Table 6.

For propagation delay compensation, in Figure 3, the delay t_k^{down} is expressed as follows:

$$t_k^{\text{down}}(t) = \Delta t_k + \tau_{tx}^s + \frac{R_k^{\text{down}}(t)}{c} + \tau_{\text{down}}^{\text{ion}} + \tau_{rx}^m, \quad (1)$$

where Δt_k consists of the time error of the 1PPS produced by GPS receivers of satellite and terminal, as well as the synchronization errors of local 1PPS generators. The speed of electromagnetic radiation varies, depending on temperature, pressure, and relative humidity, as it passes through the troposphere. Then the tropospheric time-delay results, also known as tropospheric errors. Due to tropospheric errors being independent of carrier frequency, the errors can be counteracted between downlink and uplink.

Parameters	Definition
τ_{tx}^{s}	The transmission delay of satellite transmitter
τ_{rx}^{s}	The transmission delay of satellite receiver
τ_{tx}^{m}	The transmission delay of terminal transmitter
τ_{rx}^{m}	The transmission delay of terminal receiver
τ_{down}^{ion}	The ionospheric downlink time-delay
τ_{up}^{ion}	The ionospheric uplink time-delay
c	The velocity of electromagnetic wave in vacuum
$R_k(\Delta t)/c$	The time that the pilot travels for the varied distance between satellite and terminal when terminal estimates the propagation delay and waits to transmit

The measurement accuracy of the t_k^{down} is decided by the tracking loop bandwidth (Hz) of phase lock loops (PLL), carrier to noise power expressed as a ratio (Hz), and period of the PN code (seconds). The standard deviation (1-sigma) for t_k^{down} is computed as follows [12]:

$$\sigma\left(t_k^{\text{down}}\right) \approx T_c \sqrt{\frac{B_n}{2C/N_0}} \text{ (s)}, \tag{2}$$

where T_c is the code duration, B_n is the tracking loop bandwidth, and C/N_0 is carrier to noise power expressed as a ratio (Hz).

Normally, $\sigma(t_k^{\text{down}})/T_c < 0.05$ [12], so the code rate is 5 Mchip/s, and then the measurement accuracy of the t_k^{down} will be less than 10 ns. The measurement accuracy of the terminals is similar to the satellite.

The ionospheric time-delay is computed as follows [12]:

$$\tau_{\text{down}}^{\text{ion}} = \frac{1}{\sin\left(\phi'\right)} \frac{40.3}{\left(f_c^{\text{down}}\right)^2 \cdot c} \cdot \text{TEC (s)}, \tag{3}$$

where f_c^{down} is the downlink carrier frequency of the signal, ϕ' is the elevation angle at the ionospheric pierce point, c is the velocity of electromagnetic wave in vacuum, and TEC is the total electron content. The GPS navigation message will provide $\tau_{\text{down}}^{\text{ion}}$.

To achieve QS-CDMA access, the terminals estimate the uplink propagation delay through t_k^{down} and transmit signals before next 1PPS in Figure 3. The estimation of the uplink propagation delay is computed as follows:

$$t_k^{\text{up}}(t) = \tau_{tx}^m + \frac{R_k^{\text{up}}(t)}{c} + \tau_{\text{up}}^{\text{ion}} + \tau_{rx}^s, \tag{4}$$

where

$$\frac{R_k^{\text{up}}(t)}{c} = \frac{R_k^{\text{down}}(t)}{c} + \frac{R_k(\Delta t)}{c}. \tag{5}$$

In the above equations, $R_k(\Delta t)/c$ is the time that the pilot travels for the varied distance between satellite and terminal when terminal estimates the propagation delay and waits to transmit.

Substituting (1) and (5) into (4), t_k^{up} is given by

$$t_k^{\text{up}}(t) = t_k^{\text{down}}(t) - \Delta t_k + \frac{R_k(\Delta t)}{c} + \tau_{tx}^m - \tau_{rx}^m + \tau_{rx}^s$$
$$- \tau_{tx}^s + \tau_{\text{up}}^{\text{ion}} - \tau_{\text{down}}^{\text{ion}}, \tag{6}$$

where $\tau_{tx}^m - \tau_{rx}^m$ is the delay time difference between transmitter and receiver of terminal, which should be measured and be easy to eliminate in advance, $\tau_{rx}^s - \tau_{tx}^s$ is the delay time difference between transmitter and receiver of satellite, and it is also easy to eliminate in advance, and $\tau_{\text{up}}^{\text{ion}} - \tau_{\text{down}}^{\text{ion}}$ is the ionospheric time-delay difference between uplink and downlink.

In above equation, the parameters are decided for the accuracy of t_k^{up}. Hence, we analyze the precision of the parameters.

3.2.1. Time Error Δt_k. The local clock synchronization is similar to PLL. One metric that is normally used to determine if loss of lock has occurred in a PLL is the total phase jitter, which is defined as [12]

$$\sigma_\varphi = \sqrt{\sigma_{\varphi_0}^2 + \sigma_v^2 + \sigma_A^2} + \frac{\sigma_{\varphi_d}}{3} \leq 15 \text{ deg}, \tag{7}$$

where σ_{φ_0} represents the standard deviation (1-sigma) thermal noise in degrees, σ_v represents the 1-sigma vibration-induced oscillator jitter in degrees, σ_A represents Allan variance-induced oscillator jitter in degrees, and σ_{φ_d} represents dynamic stress error in the PLL tracking loop.

For the local clock synchronization, oscillator jitter is the prime jitter. The phase jitter σ_v caused by the receiver clock depends on the quality of the clock. A close-form expression for phase jitter due to clock error in a third-order PLL can be given by [13]

$$\sigma_v^2 = \frac{0.9048(2\pi)^3 h_{-4}}{B_L^3} + \frac{0.8706(2\pi)^2 h_{-3}}{B_L^2}$$
$$+ \frac{1.2566(2\pi) h_{-2}}{B_L}, \tag{8}$$

where B_L is one-sided PLL loop bandwidth. h_{-4}, h_{-3}, and h_{-2} are clock's coefficients, which can be determined experimentally in [13]. Because their effect on phase jitter is minimal, h_{-1} and h_0 are neglected. The coefficients are shown in Table 7. The phase jitter values as a function of B_L computed using this model are shown in Figure 7.

The loop order is sensitive to the same order of dynamics, and the loop bandwidth must be wide enough to accommodate these higher-order dynamics. The first order is sensitive to velocity stress, second order to acceleration stress, and third order to jerk stress. For the local clock synchronization, the oscillator jitter is the prime jitter. The thermal noise and dynamic stress error have less effect on the time jitter of the local clock synchronization, in Figure 7, and increasing the one sided PLL loop bandwidth reduces the phase jitter; then the oscillator jitter can be neglected. So Δt_k is decided by the

TABLE 7: Coefficients in TCXO and OCXO clock error models.

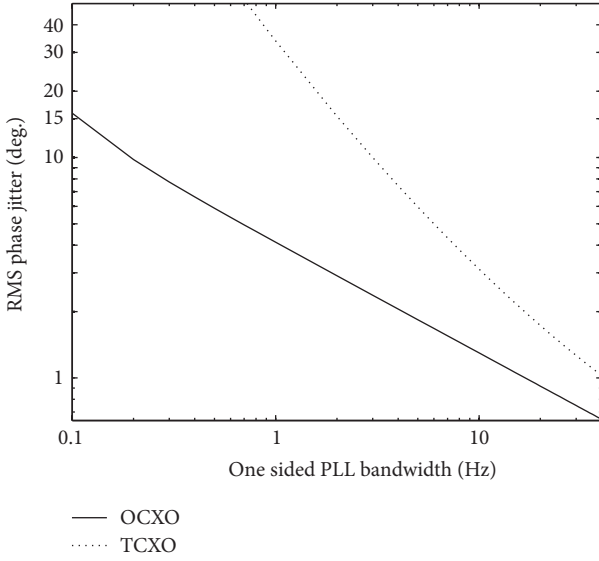| Coefficient	TCXO	OCXO
h_{-2}	9.6×10^{-4}	6.5×10^{-4}
h_{-3}	6×10^{-3}	9×10^{-7}
h_{-4}	6×10^{-4}	1×10^{-7}

— OCXO
...... TCXO

FIGURE 7: Phase jitter from clock.

time error of the 1PPS produced by GPS receivers of satellite and terminal and computed as follows:

$$\Delta t_k \approx \sqrt{100^2 + 10^2} = 100.5 \text{ ns.} \tag{9}$$

The FPGA implementation based on the local clock synchronization block in Figure 6 operated at a 40 MHz clock speed. TCXO was as a master clock and then the results of experiment are that Δt_k varied between 75 ns and 125 ns in a short time.

3.2.2. The Delay Time Difference between Transmitter and Receiver of Terminal $\tau_{tx}^m - \tau_{rx}^m$. The delay time difference is the parameters of device design and can generally be controlled below 50 ns.

3.2.3. The Delay Time Difference between Transmitter and Receiver of Satellite $\tau_{rx}^s - \tau_{tx}^s$. The delay time difference can generally be controlled below 30 ns.

3.2.4. The Ionospheric Time-Delay Difference between Uplink and Downlink $\tau_{up}^{ion} - \tau_{down}^{ion}$. At the carrier center frequency, τ_{down}^{ion} is approximately equal to 30 ns and computed by (3). At the same time, τ_{up}^{ion} is decided by the uplink carrier frequency. In general, the ionospheric time-delay of the maximum

TABLE 8: Main parameters of compensation analysis.

Parameters	Definition
L	The distance between the satellite and the terminal
t	The time when the satellite is visible to the terminal
f_d	The carrier Doppler shift that is the carrier frequency offset due to the motion of the satellite
$\dot{f_d}$	The carrier Doppler shift rate that is the rate of varying carrier frequency due to the motion of the satellite

ionospheric frequency is 150 ns. $\tau_{up}^{ion} - \tau_{down}^{ion}$ can be computed as follows:

$$
\begin{aligned}
\tau_{up}^{ion} - \tau_{down}^{ion} &\approx \frac{40.3}{\left(f_c^{up}\right)^2 \cdot c} \cdot \text{TEC} - \frac{40.3}{\left(f_c^{down}\right)^2 \cdot c} \cdot \text{TEC} \\
&= \frac{\left(f_c^{down}\right)^2 - \left(f_c^{up}\right)^2}{\left(f_c^{up}\right)^2 \cdot \left(f_c^{down}\right)^2 \cdot c} \cdot 40.3 \cdot \text{TEC} \\
&\approx 0.1 \cdot \frac{40.3}{c} \cdot \text{TEC.}
\end{aligned}
\tag{10}
$$

Thus, the ionospheric time-delay difference is less than 15 ns.

3.2.5. The Time Light Travels for the Varied Distance between Satellite and Terminal $R_k(\Delta t)/c$. The value is the time that electromagnetic wave travels for the varied distance between satellite and terminal when terminal estimates the propagation delay and waits to transmit. The accuracy of varied distance delay estimation can be achieved within 100 ns, so $R_k(\Delta t)/c$ can be precise to compensate. The analysis will be specifically discussed in Section 3.3.

In short, the estimation error of the uplink propagation delay is computed as follows:

$$
\begin{aligned}
&\sqrt{10^2 + 100^2 + 10^2 + 30^2 + 50^2 + 15^2 + 100^2} \\
&= 154 \text{ ns.}
\end{aligned}
\tag{11}
$$

The prime estimation error is the average time error of the 1PPS produced by terminal receivers, and the current production showed that jumps are much less than 100 ns [4]. Thus, the novel system structure based on GPS 1PPS is shown to code Doppler shift which is less than 1 chip at 5 Mchip/s.

3.3. Doppler Shift and Propagation Delay Compensation. In this paper, we assume that orbit altitude is 1000 km and maximum elevation angle is 90 degrees, so the visibility time is approximately 9 minutes. Some parameters are defined in Table 8.
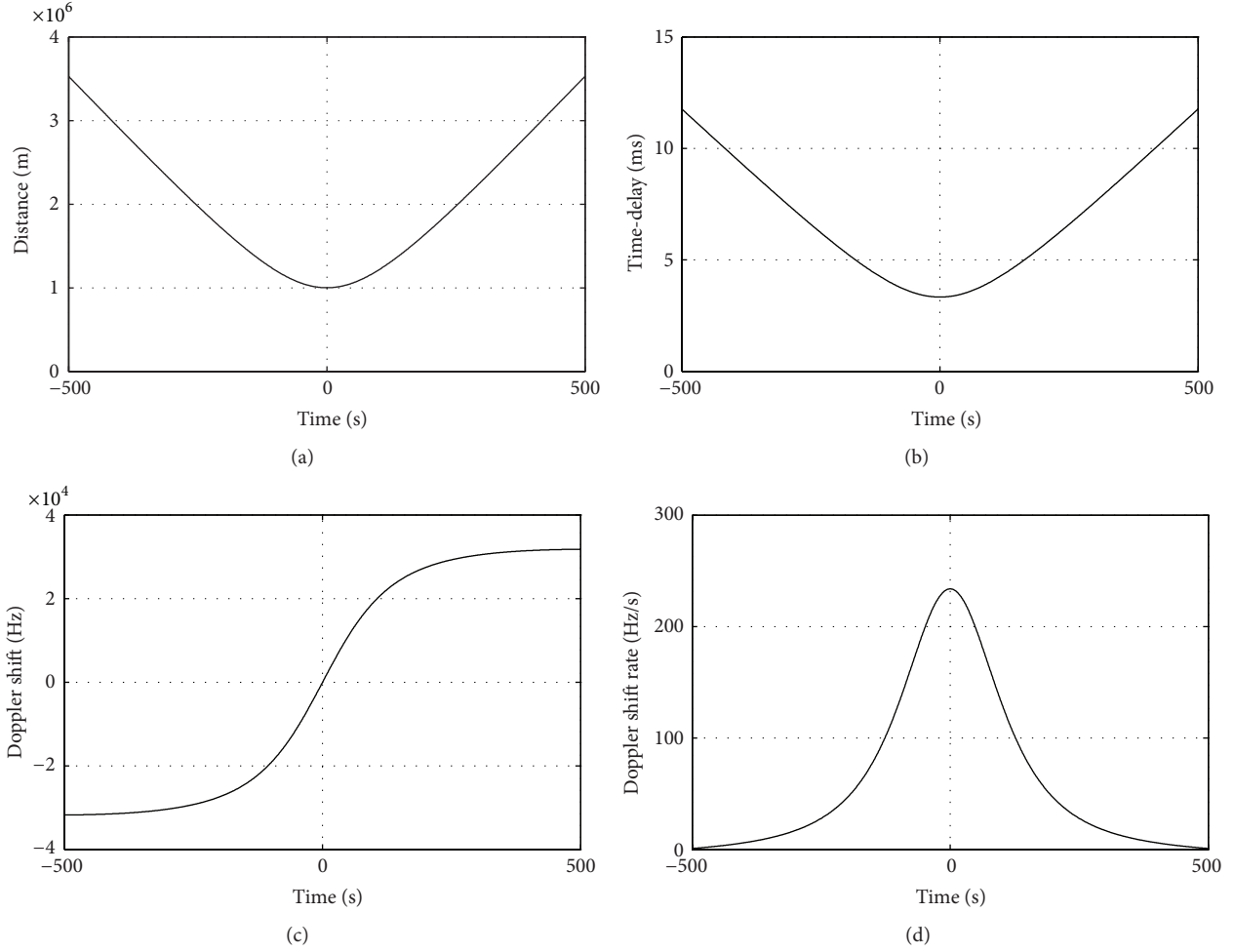
FIGURE 8: (a) Distance versus time, (b) time-delay versus time, (c) Doppler shift versus time, and (d) Doppler shift rate versus time.

3.3.1. Carrier Doppler Shift and Propagation Delay.

When the elevation angle is 90 degrees, we define that t is 0 seconds. The carrier Doppler shift is computed as follows [8]:

$$
\Delta\varphi = \varphi(t) - \varphi(t_0),
$$
$$
\Delta\theta = \arccos\left(\frac{R_E}{r}\cos\theta_{\max}\right) - \theta_{\max},
$$
$$
f_d = -\frac{f_c}{c}\frac{R_E r \sin(\Delta\varphi)\cos(\Delta\theta)\cdot\omega(t)}{\sqrt{R_E^2 + r^2 - 2R_E r \cos(\Delta\varphi)\cos(\Delta\theta)}},
\tag{12}
$$

where $\Delta\varphi$ is the angular distance measured along the ground trace, $\varphi(t)$ and $\varphi(t_0)$ are different measured points on the surface of earth along the ground trace, c is the velocity of electromagnetic wave in vacuum, f_c is carrier frequency, R_E is earth radius, and r is the distance between geocenter and satellite and is equal to the sum of earth radius and circular orbit altitude. $\theta_{\max}$ is a maximum elevation angle and $\omega(t)$ is the angular velocity of the satellite in the ECF frame. We assume that the orbit is a circular orbit, the maximum elevation angle is 90 degrees, and a simplified expression for Doppler shift can be given by

$$
V = \sqrt{\frac{R_E^2}{r}\cdot g},
\tag{13}
$$
$$
\gamma = \frac{V\cdot t}{r},
\tag{14}
$$
$$
L = \sqrt{R_E^2 + r^2 - 2R_E r \cos(\gamma)},
\tag{15}
$$
$$
f_d = \frac{V\cdot f_c \cos(\gamma)}{c},
\tag{16}
$$

where V is the velocity of the satellite for a circular orbit. Then $V\cos(\gamma)$ is the radial velocity. c is the velocity of electromagnetic wave in vacuum. g is the acceleration of gravity. γ is the angle between the direction of incoming signal and the direction of the velocity V; r is equal to the sum of earth radius and circular orbit altitude. The distance, carrier Doppler shift, and Doppler shift rate as a function of t computed using this model are shown in Figure 8.

In Figure 8(a), we can see the relationship between propagation delay and time. In Figure 8(b), we can see the relationship between propagation time-delay and time. In Figure 8(c), we can see the relationship between carrier Doppler shift and time. In Figure 8(d), we can see the relationship between carrier Doppler shift rate and time. We assume that satellite begins to be in vision when t is -450 s. At this point, the value for the distance L, the time-delay, and the Doppler shift are all the maximum, and the Doppler shift rate is the minimum. At the same time, the $R_k(\Delta t)/c$ will be achieved in 10 microseconds (μs) level, and the chip error will be more than 50 chips. When t is 0 s, the $R_k(\Delta t)/c$ will be achieved in 100 ns level, and the chip error will be less than one chip.

3.3.2. The Analysis and Estimation Method to Carrier Doppler Shift and $R_k(\Delta t)/c$. We suggest using the following method to estimate carrier Doppler shift and $R_k(\Delta t)/c$.

Through the estimation of downlink carrier and chip frequency offered by receiver's tracking loop, the uplink carrier and code Doppler shift can be accurately computed. The $V\cos(\gamma)$ can be computed by the estimation of uplink frequency and updated every signal period whose rate is 5 kHz. The accuracy of estimation can be achieved to 100 ns.

Firstly, we have to analyze the terminal receiver's FLL, PLL, and DLL tracking loop measurement errors that directly affect the accuracy of uplink Doppler shift and propagation delay compensation.

We assume that the received signal power is -120 dBmW; noise power spectral density N_0 is -175 dBmW. The tracking loop measurement errors can be computed from the formulas in [12] and be shown in Figure 9.

In Figure 9(a), we can see the relationship between total frequency lock loop (FLL) jitter and time. In Figure 9(b), we can see the relationship between FLL dynamic stress and time. In Figure 9(c), we can see the relationship between total PLL jitter and time. In Figure 9(d), we can see the relationship between phase lock loop (PLL) dynamic stress and time. In Figure 9(e), we can see the relationship between total code tracking loop (DLL) jitter and time. In Figure 9(f), we can see the relationship between DLL dynamic stress and time. From Figure 9, we can see that the terminal receiver's FLL, PLL, and DLL tracking loop measurement errors have less effect on Doppler shift compensation at high C/N_0. Therefore, as long as the carrier loop remains stable, the code loop experiences negligible dynamic stress.

Secondly, we will analyze the frequency deviation caused by the TCXO with frequency stability of ±0.5 ppm or OCXO with frequency stability of ±0.05 ppm. The signal conditioned RF signals are down-converted to an intermediate frequency (IF) using signal mixing frequencies from local oscillators. The local oscillators are derived from the reference oscillator by the frequency synthesizer, based on the TCXO or OCXO. At downlink carrier frequency which is 1.5 GHz, the most frequency deviation of the frequency synthesizer, caused by TCXO, is ±750 Hz, and the most frequency deviation caused by OCXO is ±75 Hz. After the mixing process, at the IF, this frequency deviation is a fixed bias that will be

additional carrier Doppler shift. From Figure 8, we can see that the maximum carrier Doppler shift rate is far less than 1/2 data rate in the time when signal is transmitted from the transmitter of satellite to the receiver of terminal. The tracking loop measurement error is less than 1 Hz. We assume that the satellite and terminal use the same TCXO or OCXO. The estimation error of uplink carrier Doppler shift can be given as follows:

$$
\begin{aligned}
\text{TCXO: } & \sqrt{750^2 + 750^2 + 1^2} = 1061 \text{ Hz,} \\
\text{OCXO: } & \sqrt{75^2 + 75^2 + 1^2} = 106 \text{ Hz.}
\end{aligned}
\tag{17}
$$

Therefore, this frequency deviation is less than 1/2 data rate, and it will be easy to be acquired. Thus, it has less effect on increasing the complexity of satellite's receiver.

Finally, through the estimation of downlink carrier and chip frequency offered by receiver's tracking loop, we can compute the $V\cos(\gamma)$ by (16) and estimate the varied distance $R_k(\Delta t)$. The estimation of the varied distance $R_k(\Delta t)$ updates every signal period whose rate is 5 kHz.

We compute the $V\cos(\gamma)$ by (16) and estimate the varied distance $R_k(\Delta t)$. The estimation error of the varied distance $R_k(\Delta t)$ using this model is shown in Figures 10 and 11. It consists of theoretic estimation error, estimation error with TCXO and estimation error with OCXO. The theoretic estimation means that the frequency deviation is 0Hz. Because the terminals in the great disaster region or sensors in remote region are stationary or low velocity moving, it results that the carrier Doppler shift caused by motion is far less than the frequency deviation caused by the oscillator. Thus we will mainly analyze the frequency deviation caused by the oscillator. The estimation of the varied distance $R_k(\Delta t)$ updates every signal period whose time is 200 μs.

In Figure 10(a), we can see the relationship between theoretic estimation error and time. Because estimation of the varied distance $R_k(\Delta t)$ updates every signal period, the theoretic errors can fluctuate caused by quantization error. In Figure 10(b), we can see the relationship between estimation error with TCXO and time. In Figure 10(c), we can see the relationship between estimation error with OCXO and time. The time is between -450 s and -449 s.

In Figure 11(a), we can see the relationship between theoretic estimation error and time, where theoretic estimation means that the frequency deviation is 0 Hz. In Figure 11(b), we can see the relationship between estimation error with TCXO and time. In Figure 11(c), we can see the relationship between estimation error with OCXO and time. The time is between -1 s and 0 s.

From Figure 10(a), when t is -450 s, we can get the sum of varied distance estimation error in one second, and the accuracy of compensation for $R_k(\Delta t)/C$ will be achieved in 1 femtosecond (fs) level. From Figure 11(a), when t is 0 s, then the accuracy of compensation will be achieved in 10 fs level. From Figures 10(b) and 11(b), the accumulative estimation error with TCXO is 240 meters (m) in one second, and the error of compensation is 800 ns. From Figures 10(c) and 11(c), the accumulative estimation error with OCXO is 22 m in one second, and the error of compensation is 74 ns. It is less than
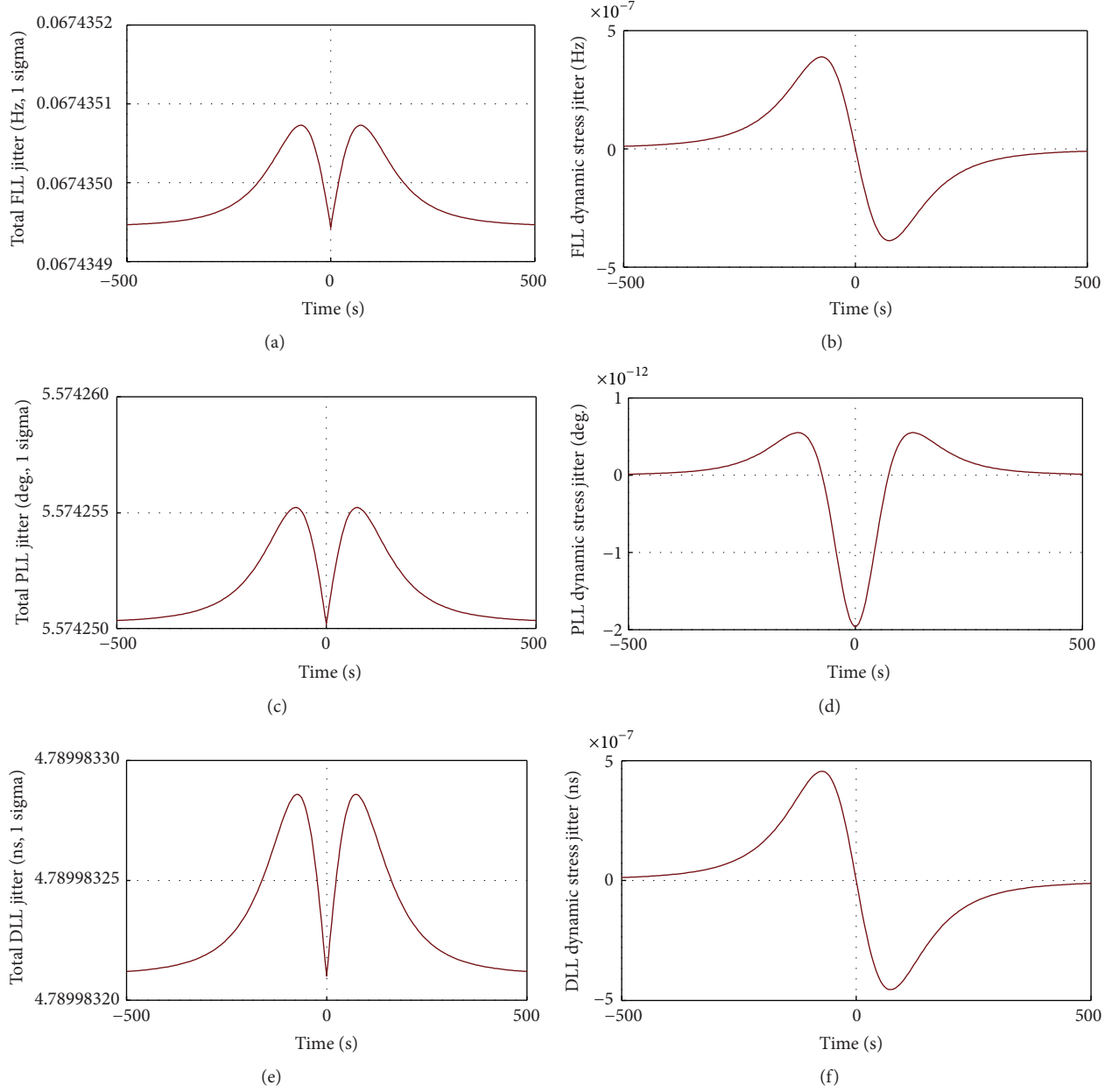
FIGURE 9: Tracking loop measurement errors.

100 ns, which has been required in Section 3.2. Therefore, this frequency deviation has significant effect on the estimation error of the varied distance $R_k(\Delta t)$.

In the visibility time, which is approximately 9 minutes, estimation errors through simulations are shown in Figure 12.

In Figure 12(a), we can see the relationship between theoretic accumulative estimation error in one second and time. In Figure 12(b), we can see the relationship between accumulative estimation error in one second with TCXO and time when estimation error of uplink carrier Doppler shift is 1200 Hz. In Figure 12(c), we can see the relationship between accumulative estimation error in one second with OCXO and time when estimation error of uplink carrier Doppler shift is 110 Hz. The time is between −450 s and 450 s. In Figure 12(d),

we can see the relationship between accumulative estimation error and estimation error of uplink carrier Doppler shift.

From Figures 12(a), 12(b), and 12(c), we can see that the carrier Doppler shift rate has effect on the estimation error of the varied distance $R_k(\Delta t)$, but the error is only 4.7 millimetres (mm) when carrier Doppler shift rate is the maximum.

From Figure 12(d), we can see that the more estimation error of uplink carrier Doppler shift is, the more estimation error of the varied distance $R_k(\Delta t)$ we will endure. Therefore, the frequency stability of oscillator has significant effect on the estimation error of the varied distance $R_k(\Delta t)$.

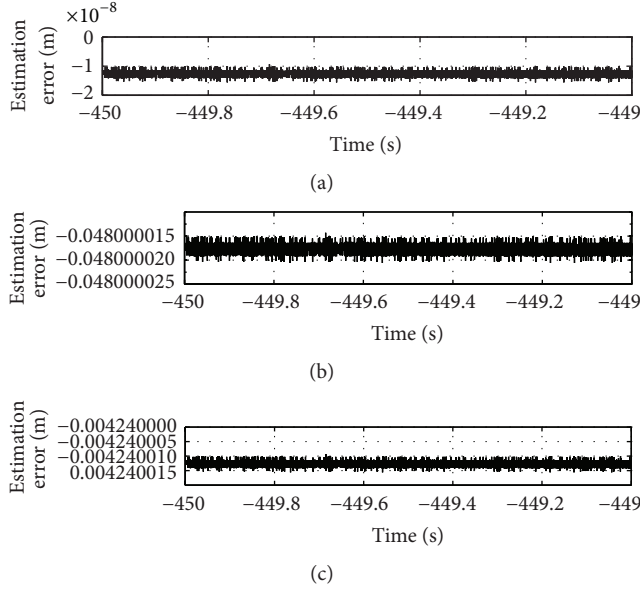From the above analysis, carrier Doppler shift and propagation delay compensation of terminal, based on

FIGURE 10: (a) Theoretic estimation error, (b) estimation error with TCXO, and (c) estimation error with OCXO.
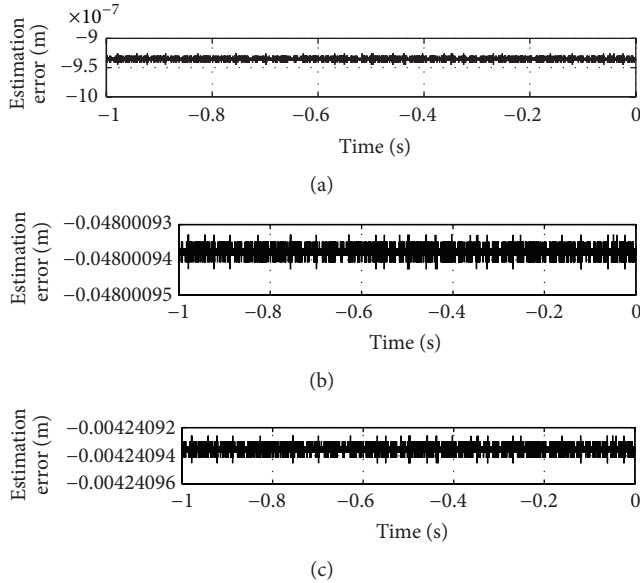

FIGURE 11: (a) Theoretic estimation error, (b) estimation error with TCXO, and (c) estimation error with OCXO.

the OCXO with frequency stability of ±0.05 ppm, can match the requirements of the QS-CDMA system. Because the prime estimation error is the average time error of the 1PPS produced by terminal receivers, the current production showed that jumps are much less than 100 ns [4]. Through (11), it results that the OCXO with frequency stability of ±0.1 ppm can also meet the requirements for the clock synchronization time error in practice.

3.4. Analysis of Error Probability. The QS-CDMA sensor data collection system proposed in this paper mainly focuses on

the following applications: emergency, marine research, and forest fire disaster. For emergency, such as earthquake, people use terminals to transmit safety confirmation in the safety and open area. For marine research, the oceanographic buoys are scattered distribution in the vast ocean. For forest fire disaster, we recommend that the sinks placed in high or open place collect information from sensors, and the sinks transmit information of forest to the LEO satellite. Therefore, the satellite channel can be considered that there is a line-of-sight (LOS), which is a dominant stationary signal component.

BER performance in the presence of additive white Gaussian noise (AWGN) and cochannel interference is derived.

Through the BPSK modulation, the jth user transmitted signal can be represented as

$$s_T^j(t) = \sqrt{P_j} \sum_{k=-\infty}^{+\infty} c_k^j \cdot d^j \cos\left(\omega_j t + \phi_j\right), \tag{18}$$

where P_j is the jth user transmitter power, c_k^j is the kth chip of the code sequence with length N for the jth user, d^j is the transmitted symbols of the jth user, ω_j is the jth user carrier angular frequency, and ϕ_j is the initial phase of the jth user.

The received signal at the demodulator input can be represented as

$$s_R(t) = \sum_{j=1}^{M} s_T^j(t) + n(t), \tag{19}$$

where $n(t)$ is the AWGN.

The received signal after down-converting is filtered with a chip matched filter. When the carrier frequency offset is not concerned, the signal after being sampled at the chip rate can be simplified as

$$s_R^j(k) = \left(\sum_{j=1}^{M} s_T^j(k)\right) \cdot c_k^j + n'(k), \tag{20}$$

where $s_R^j(k)$ is the kth output sample of the chip matched filter, $s_T^j(k)$ is the kth sample of the jth user transmitted signal, c_k^j is the kth chip of PN code for the jth user, and $n'(k) = n(k) * c_k^j$.

In [1], the probability of error for QPSK has been derived. We can use the same method to derive the BER of BPSK. It can be shown that, supposing that all the 2^{M-1} interference data patterns are equally distributed, the probability of error for the lth user in QS-CDMA system, when $2E_b/N_0 \le N^2/[\mu_l^i \cdot (M-1)]$, can be given as follows:

$$P_e^l = Q\left(\sqrt{\frac{2E_b/N_0}{1 + ((M-1)/2N^2)\,\mu_l^i\,(2E_b/N_0)}}\right). \tag{21}$$
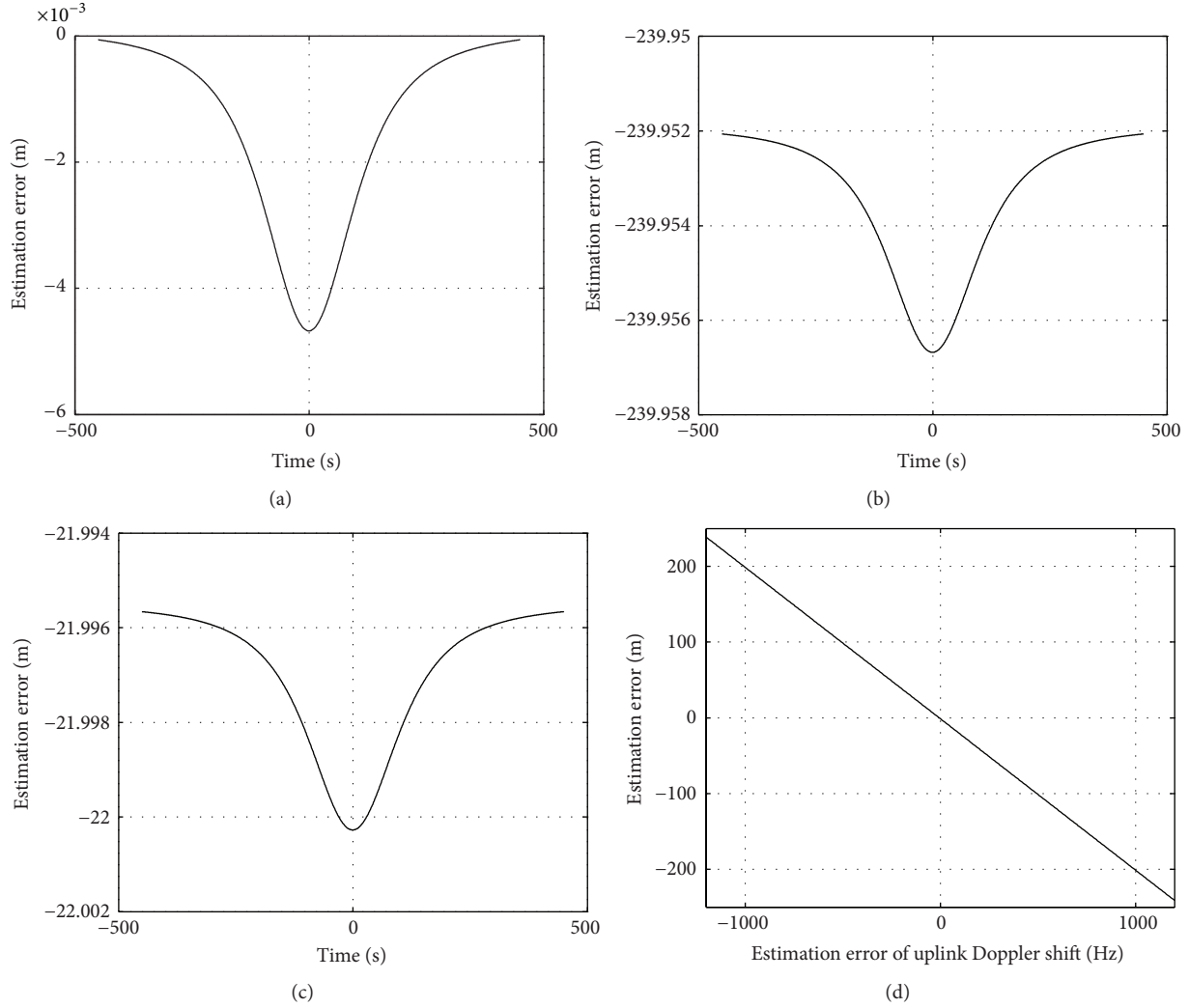
FIGURE 12: (a) Theoretic estimation error, (b) estimation error with TCXO, (c) estimation error with OCXO, and (d) estimation error versus estimation error of uplink Doppler shift.

Define now

$$Q(x) = \frac{1}{\sqrt{2\pi}} \int_x^\infty e^{(-y^2/2)} dy,$$

$$\mu_l^i = \frac{1}{M-1} \sum_{j=1, j \neq l}^M \left[\alpha_{j,l} C_{i,i}^{j,l} \right]^2,$$

$$\alpha_{j,l} = \sqrt{\frac{P_j}{P_l}}, \quad (22)$$

$$C_{i,i}^{j,l} = C_{i,i}^{j,l} \left(2\pi\Delta f, \Delta\tau, \Delta\phi, 0, (N-1) T_c \right)$$

$$= \sum_{t=0}^{(N-1)} \sum_{k=0}^{N-1} \left\{ c_k^j \cdot c_k^l (\Delta\tau) \right\} \cdot \cos\left(2\pi\Delta f \cdot t \cdot T_c + \Delta\phi \right),$$

where E_b/N_0 is the energy per bit to thermal noise density ratio. M is the number of users. N is the length of m-sequence. $\alpha_{j,l}$ is the power ratio between the jth user and lth

user. $C_{i,i}^{j,l}$ is the cross-correlation factors of the In-Phase (I) branch. c_k^j is the kth chip of PN code for the jth user. Δf is the residual carrier frequency offset. $\Delta\tau$ is the PN code offset. $\Delta\phi$ is the phase offset of carrier. T_c is the code duration.

According to the analysis of Section 3, we assume that Δf is varied over a range of about 2 kHz; $\Delta\tau$ is varied within a range of ± 1 chip. Thus every user selects a shift-m-sequence, whose code phase interval between one user and the other is greater than or equal to 3 chips.

Figure 13 shows the theory BER curves of three systems. The Asynchronous Code Division Multiple Access (ACDMA dots) approaches a constant for different number of users. When the number of users is much more, the BER performance of ACDMA is so bad that the data of lth user cannot be demodulated. The QSCDMA-I (dashed line) uses Gold sequence to spread spectrum. We can see that the BER performance of the QSCDMA-I is much better than that of the ACDMA. Unfortunately, with the increase of the number of users, the Gold sequences lose a lot of
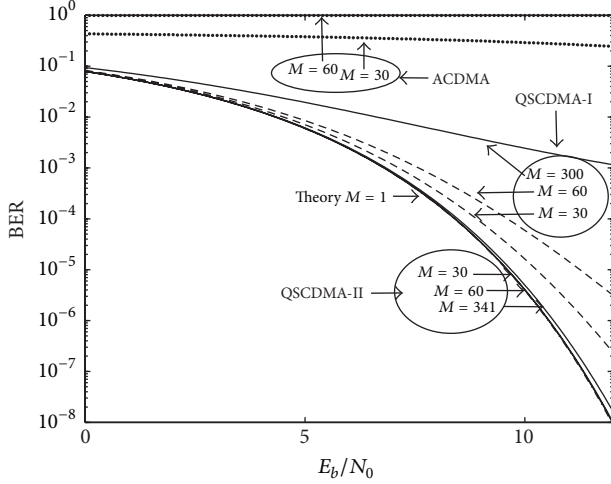
FIGURE 13: BER curves of ACDMA, QSCDMA-I, and QSCDMA-II.

the BER performance. The QSCDMA-II (continuous line) uses shift-m-sequence to spread spectrum. Because $\Delta\tau$ is varied within a range of ± 1 chip, the maximum number of users in the QSCDMA-II system is 341. We can see that the BER performance of the QSCDMA-II is much better than that of the QSCDMA-I.

From Figure 13, we can see that the loss of BER performance in QSCDMA-II system increases much slower than in QSCDMA-I system as the number of users grows. Therefore, the MAI of QSCDMA-II system is obviously decreased.

4. Simulation and Experiment Results

In this section, we present simulation and experiment results in order to validate the performance of QS-CDMA system. BER performance in the presence of additive white Gaussian noise (AWGN) and cochannel interference is analyzed.

We assume that the power of all users is equal. There are 341 users who are transmitting data at the same time. Because $\Delta\tau$ is varied within a range of ± 1 chip, in order to avoid the self-interference of shift-m-sequences, the maximum number of users in the QSCDMA-II system is 341. So every user selects a shift-m-sequence, whose code phase interval between one user and the other is equal to 3 chips. There is no user collision in the same code phase. Δf is varied over a range of about 2 kHz. The simulation results are shown in Figure 14.

Figure 14 shows that the simulation results of QSCDMA-II are in accordance with the theoretical prediction. Therefore, the uplink preamble of the system selects such shift-m-sequence that the system can achieve much better BER performance and serve more users. The MAI of the system can be obviously decreased.

From simulation results, we can see that the performance of BER is excellent, when the power of all users is equal. Then we mainly consider the situations that the power of every user is not equal by experiments. The experiment environment consists of several terminals and one satellite simulator. The main functions of the satellite simulator are to simulate
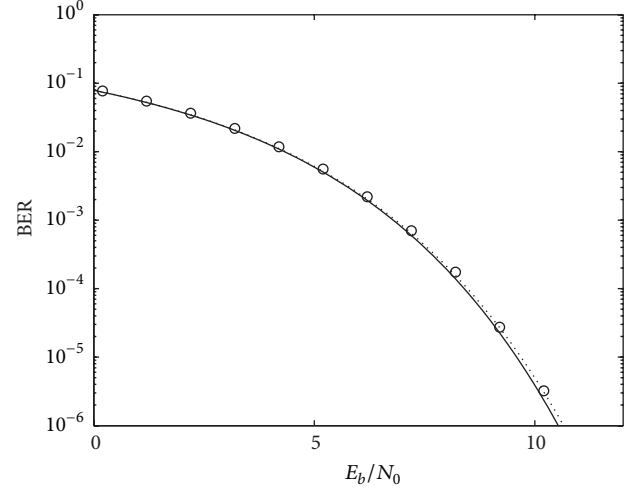

——— 1 user theory
.... 341 users theory
o   341 users simulation results

FIGURE 14: QSCDMA-II simulation BER.

TABLE 9: Several situations.

Number	Situation
A	The power of 1 jamming user is 12 dB higher than main user
B	The power of 1 jamming user is 14 dB higher than main user
C	The power of 2 jamming users is 12 dB higher than main user
D	The power of 2 jamming users is 14 dB higher than main user
E	The power of 7 jamming users is 5 dB higher than main user
F	The power of 7 jamming users is 6 dB higher than main user
G	The power of 15 jamming users is 5 dB higher than main user
H	The power of 15 jamming users is 6 dB higher than main user

the changes of Doppler shift, Doppler shift rate, and propagation delay. We tested the performance of BER in several situations. The situations are shown in Table 9. We also assume that $\Delta\tau$ is varied within a range of ± 1 chip, Δf is varied over a range of about 2 kHz, and every user selects a shift-m-sequence, whose code phase interval between one user and the other is greater than or equal to 3 chips. We record the BER of the main user at low E_b/N_0 and assume that other users are strong jamming. The results of experiment are shown in Table 10.

From Table 10, we compare numbers 1, 2, and 3 with numbers 7, 8, and 9 and can see that the BER performance of QS-CDMA system is a little better than A-CDMA system. We compare numbers 4, 5, and 6 with numbers 11, 12, and 13 and can see that the BER performance of QS-CDMA

TABLE 10: Experiment results.

Number	E_b/N_0	System	Situation	BER
1	4 dB	A-CDMA	A	0.018249
2	4 dB	A-CDMA	C	0.019617
3	4 dB	A-CDMA	F	0.019955
4	4.5 dB	A-CDMA	A	0.012103
5	4.5 dB	A-CDMA	C	0.013560
6	4.5 dB	A-CDMA	E	0.014162
7	4 dB	QS-CDMA	A	0.016380
8	4 dB	QS-CDMA	C	0.016860
9	4 dB	QS-CDMA	F	0.019129
10	4 dB	QS-CDMA	H	0.023877
11	4.5 dB	QS-CDMA	B	0.010924
12	4.5 dB	QS-CDMA	D	0.011111
13	4.5 dB	QS-CDMA	E	0.013143
14	4.5 dB	QS-CDMA	F	0.013247
15	4.5 dB	QS-CDMA	G	0.016321
16	4.5 dB	QS-CDMA	H	0.016555

system is also a little better than the A-CDMA system. The prime reason of this phenomenon, which is different from the results in Figure 14, is that the power of jamming users is far more than main user. Thus the power control is important in QS-CDMA system, too.

5. Conclusions

In the paper, a quasisynchronous CDMA uplink access technique in the LEO satellite has been presented and discussed. From the analysis of clock synchronization time error based on GPS, the novel system structure based on GPS 1PPS is shown to code offset which is less than 1 chip at 5 Mchip/s, and the effect of the multiple-access interference can be greatly reduced. The effect on Doppler compensation, caused by the frequency stability of terminal's oscillator, is analyzed emphatically. It results that, by Doppler compensation, we can reduce the time of acquisition and the complexity of implementation in satellite. These methods are used to guide the specific hardware implementation of the QS-CDMA. The FPGA implementation can be proved that Doppler compensation can achieve the requirements of QS-CDMA system, the probability of error is drastically reduced compared to A-CDMA system, and the number of users is drastically increased. The QS-CDMA sensor data collection system proposed in this paper mainly focuses on the following applications: emergency, marine research, and forest fire disaster. The QS-CDMA system is easy to implement, use in remote, and collect data from more sensors. Meanwhile, the system can respond quickly to emergencies.

Conflict of Interests

The authors declare that there is no conflict of interests regarding the publication of this paper.

References

[1] R. De Gaudenzi, C. Elia, and R. Viola, "Bandlimited quasi-synchronous CDMA: a novel satellite access technique for mobile and personal communication systems," *IEEE Journal on Selected Areas in Communications*, vol. 10, no. 2, pp. 328–343, 1992.

[2] R. De Gaudenzi, G. Gallinaro, G. Caire et al., "ESA satellite wideband CDMA radio transmission technology for the IMT-2000/UMTS satellite component: features and performance," in *Proceedings of the IEEE Global Telecommunication Conference (GLOBECOM '99)*, pp. 2699–2703, December 1999.

[3] Z.-Y. Zhang and L.-F. Lai, "A practical slotted quasi-synchronous CDMA access system for LEO micro-satellite short message transmission," in *Proceedings of the International Conference on Communications (ICC '03)*, pp. 2114–2118, May 2003.

[4] R. M. Hambly and T. A. Clark, "Critical evaluation of the Motorola M12+ GPS timing receiver vs. the master clock at the United States Naval Observatory, Washington, DC," in *Proceedings of the 34th Annual PTTI Meeting*, pp. 109–115, 2002.

[5] T. A. Clark and R. M. Hambly, "Low cost GPS-based time and frequency products, an update," in *Proceedings of the 44th Annual PTTI Meeting*, Reston, Va, USA, November 2012.

[6] L. Arceo-Miquel, Y. S. Shmaliy, and O. Ibarra-Manzano, "Optimal synchronization of local clocks by GPS 1PPS signals using predictive FIR filters," *IEEE Transactions on Instrumentation and Measurement*, vol. 58, no. 6, pp. 1833–1840, 2009.

[7] Y. S. Shmaliy, A. V. Marienko, and A. V. Savchuk, "GPS-based optimal Kalman estimation of time error, frequency offset, and aging," in *Proceedings of the 31st Annual PTTI Meeting*, pp. 431–440, 1999.

[8] A. H. Irfan, N. Al-Dhahir, and J. E. Hershey, "Doppler characterization for LEO satellites," *IEEE Transactions on Communications*, vol. 46, no. 3, pp. 309–313, 1998.

[9] U. Cheng, W. J. Hurd, and J. I. Statman, "Spread-spectrum code acquisition in the presence of Doppler shift and data modulation," *IEEE Transactions on Communications*, vol. 38, no. 2, pp. 241–250, 1990.

[10] L. Hyoungsoo, L. Soo-In, and L. Seong-Pal, "A simple carrier frequency detection algorithm for fine compensation of Doppler shift in direct-sequence code division multiple access mobile satellite communications," in *Proceedings of the IEEE International Conference on Communications (ICC '00)*, pp. 109–112, New Orleans, La, USA, 2000.

[11] J. S. Lee and L. E. Miller, *CDMA Systems Engineering Handbook*, Artech House, 1998.

[12] E. D. Kaplan and C. Hegarty, *Understanding GPS: Principles and Applications*, Artech House, 2006.

[13] A. Razavi, D. Gebre-Egziabher, and D. M. Akos, "Carrier loop architectures for tracking weak GPS signals," *IEEE Transactions on Aerospace and Electronic Systems*, vol. 44, no. 2, pp. 697–710, 2008.